文章编号：0253-2409(2012)12-1444-10

Theoretical study on the interactions between dibenzothiophene/dibenzothiophene sulfone and ionic liquids

LÜ Ren-qing[1], LIN Jin[2], QU Zhan-qing[3]

(1. *College of Science, China University of Petroleum (East China), Qingdao* 266580, *China*;
2. *College of Chemical Engineering, China University of Petroleum (East China), Qingdao* 266580, *China*;
3. *College of Petroleum Engineering, China University of Petroleum (East China), Qingdao* 266580, *China*)

Abstract: The interactions between sulfur-containing compounds of dibenzothiophene (DBT) and dibenzothiophene sulfone ($DBTO_2$) and ionic liquids of 1-butyl-3-methylimidazolium hexafluorophosphate ($[BMIM]^+[PF_6]^-$) and 1-butyl-3-methylimidazolium tetrafluoroborate ($[BMIM]^+[BF_4]^-$) were comparatively studied by using density functional theory. The most stable structures of $[BMIM]^+[PF_6]^-$, $[BMIM]^+[PF_6]^-$-DBT, $[BMIM]^+[PF_6]^-$-$DBTO_2$, $[BMIM]^+[BF_4]^-$, $[BMIM]^+[BF_4]^-$-DBT, and $[BMIM]^+[BF_4]^-$-$DBTO_2$ systems were obtained by natural bond orbitals (NBO) and atoms in molecules (AIM) analyses. The results indicated that DBT and [BMIM] rings of $[BMIM]^+[PF_6]^-$/$[BMIM]^+[BF_4]^-$ are parallel to each other. There is a strong π-π interaction between them in terms of NBO and AIM analyses. The H1′ and H9′ involved F···H hydrogen bonding interactions may favor the formation of π-π stacking interactions. The $DBTO_2$ preferentially locates near the C2-H2 and methyl group of $[BMIM]^+$ to form O···H interactions. The predicted geometries and interaction energies imply the preferential adsorption of $DBTO_2$ on $[BMIM]^+[PF_6]^-$/$[BMIM]^+[BF_4]^-$. The $[BMIM]^+[PF_6]^-$/$[BF_4]^-$ have better extracting ability to remove $DBTO_2$ than DBT, possibly due to the larger polarity of $DBTO_2$ and stronger interactions between $[BMIM]^+[PF_6]^-$/$[BF_4]^-$ and $DBTO_2$.

Key words: density functional theory; dibenzothiophene; dibenzothiophene sulfone; ionic liquid.
CLC number: TE624 **Document code**: A

Due to the stringent environmental regulations on sulfur concentration in transportation fuels, ultra-deep desulfurization of fuels has become an important research subject. Hydrodesulfurization (HDS) at high temperature and high pressure over Mo-based catalysts is a major process in petroleum processing industry to reduce the sulfur in fuels. Unfortunately, sulfur-containing aromatic compounds (including thiophene and its derivatives) are barely removed by this process. Therefore, the extraction of sulfur-containing compounds from the fuels under mild conditions with ionic liquids is proposed[1]. The ionic liquids show good extraction ability for aromatic sulfur-containing compounds. It has been found that S-containing compounds oxidation and extraction by ionic liquids can effectively remove a large amount of S-containing compounds from fuels[2~4]. Sulfur-containing compounds are oxidized by using different oxidants to form the corresponding sulfones that can be preferentially extracted from fuel by various ionic liquids due to their increased relative polarity. Among the many types of ionic liquids studied, those based on imidazolium cations and $[BF_4]^-$ or $[PF_6]^-$ anions show high efficiency for the extraction of organic sulfur compounds. Recent efforts have been made by using theoretical methods to model the extraction of sulfur-containing compounds with ionic liquids[5~12].

Lo et al[2] firstly reported the removal of sulfur-containing compounds from light oils by a combination of both chemical oxidation and solvent extraction using the room temperature ionic liquids, 1-butyl-3-methylimidazolium hexafluorophosphate ($[BMIM]^+[PF_6]^-$) and 1-butyl-3-methylimidazolium tetrafluoroborate ($[BMIM]^+[BF_4]^-$); the oxidation reaction of DBT is displayed in Figure 1[2]. The mechanism investigation needs to be intensified to enable deeper understanding of the extraction process. To the best of our knowledge, there is no theoretical report on the investigation of interactions between DBT/$DBTO_2$ and $[BMIM]^+[PF_6]^-$/$[BMIM]^+[BF_4]^-$ ionic liquids.

Our primary purpose in this work is to study the interactions between DBT/$DBTO_2$ and $[BMIM]^+[PF_6]^-$/$[BMIM]^+[BF_4]^-$ by means of density functional approach. The different electronic and topological properties of interactions between $[BMIM]^+[PF_6]^-$/$[BMIM]^+[BF_4]^-$ and DBT/$DBTO_2$ were compared. Although the gas phase calculation may be different from the liquid state, the results obtained here give us some new insights into the interaction of $[BMIM]^+[PF_6]^-$/$[BMIM]^+[BF_4]^-$

Received date: 2012-06-28; **Received in revised form**: 2012-09-17.

Corresponding author: LÜ Ren-qing: Tel: +86-532-86984550, Fax: +86-532-86981787, E-mail: lvrq2000@163.com.

本文的英文电子版由 Elsevier 出版社在 ScienceDirect 上出版(http://www.sciencedirect.com/science/journal/18725813)。

and DBT/$DBTO_2$.

This paper was organized as follows: Different structures of $[BMIM]^+[PF_6]^-$ and $[BMIM]^+[BF_4]^-$ pairs were first optimized, and then the structures of [BMIM] interacting with $[PF_6]^-/[BF_4]^-$ and DBT/$DBTO_2$ at different binding sites were optimized and the most stable structures were selected. The NBO and AIM analyses of the most stable structures were performed. Geometries parameters, interaction energies, and topological properties of the most stable structures were discussed in detail.

1 Specification of initial geometries

A number of computational studies[13~19] have also been performed to determine the location and orientation of imidazolium based cation-$[PF_6]^-/[BF_4]^-$ pairs of the ionic liquids. The calculated results suggest that $[PF_6]^-/[BF_4]^-$ anions tend to be located near a ring C2-proton. The structures of DBT, $DBTO_2$, PF_6^-, BF_4^- anions, and $[BMIM]^+$ cation are shown in Figures 1 and 2. The $[PF_6]^-/[BF_4]^-$ anions and DBT/$DBTO_2$ have been gradually placed in different regions around imidazolium cation to form $[BMIM]^+[PF_6]^-$-DBT, $[BMIM]^+[PF_6]^-$-$DBTO_2$, $[BMIM]^+[BF_4]^-$-DBT, and $[BMIM]^+[BF_4]^-$-$DBTO_2$ for optimization.

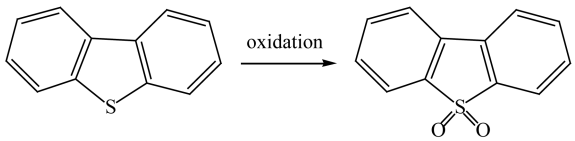

Figure 1　Oxidation of dibenzothiophene (DBT) to dibenzothiophene sulfone ($DBTO_2$)

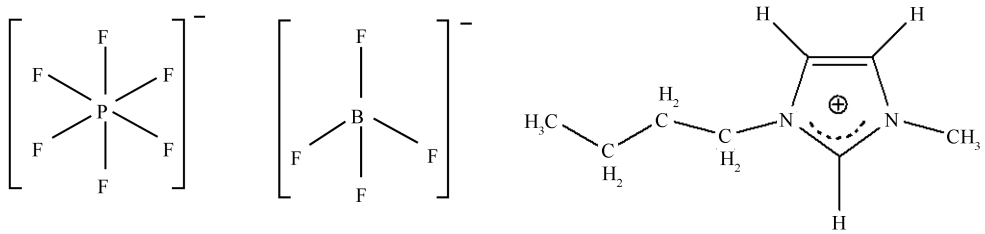

(a)　(b)　(c)

Figure 2　Structures of (a) $[PF_6]^-$, (b) $[BF_4]^-$ and (c) $[BMIM]^+$

2 Computational details

Quantum chemical calculations using gradient-corrected density functional theory were performed to investigate the interactions between $[BMIM]^+[PF_6]^-/[BMIM]^+[BF_4]^-$ and DBT/$DBTO_2$. The computational study employed the Perdew-Wang's exchange-correlation functional (PW91)[20] and a double numerical atomic basis set augmented with polarization functions (DNP) as implemented in DMol3 package[21,22]. Although PW91 functional is unable to provide a good description of dispersion interactions, GGA/PW91/DNP can give good results of interactions between conjugated systems[23]. All the stationary structures have been fully optimized without geometrical constraints. Each stationary point was checked by computing the frequencies to make sure that the optimal geometries were minima without imaginary frequency. The natural bond orbitals (NBO) analysis was obtained with 6-31++G** basis set[24]. In the NBO analysis, the second order perturbation stabilization energy $E(2)$ associated with the delocalization of $i \rightarrow j$ is estimated as

$$E(2) = \Delta E_{ij} = n_i \frac{(F_{ij})^2}{\varepsilon_j - \varepsilon_i}$$

where n_i is the donor orbital occupancy, ε_i and ε_j are the diagonal elements, and F_{ij} is the off-diagonal NBO Fork matrix element. Atoms in molecules (AIM) analyses were computed by AIM2000 to provide topological properties[25,26].

$DMol^3$ uses numerical functions that are far more complete than traditional Gaussian functions, and therefore we expect BSSE contribution to be small[27]. The interaction energies between $[BMIM]^+[PF_6]^-/[BMIM]^+[BF_4]^-$ and DBT/$DBTO_2$ were calculated according to the following expression:

$$\Delta E = [E([BMIM]^+[PF_6]^-/[BMIM]^+[BF_4]^-) + E(DBT/DBTO_2)] - E([BMIM]^+[PF_6]^-/[BMIM]^+[BF_4]^-\text{-}DBT/DBTO_2)$$

where $E([BMIM]^+[PF_6]^-/[BMIM]^+[BF_4]^-$-$DBT/DBTO_2)$ is the energies of $[BMIM]^+[PF_6]^-$-DBT, $[BMIM]^+[PF_6]^-$-$DBTO_2$, $[BMIM]^+[BF_4]^-$-DBT, and $[BMIM]^+[BF_4]^-$-$DBTO_2$. $E([BMIM]^+[PF_6]^-/BMIM]^+[BF_4]^-)$ and $E(DBT/DBTO_2)$ are the individual energies of $[BMIM]^+[PF_6]^-$, $[BMIM]^+[BF_4]^-$, DBT, and $DBTO_2$, and ΔE denotes the interaction energies between $[BMIM]^+[PF_6]^-/[BMIM]^+[BF_4]^-$ and DBT/$DBTO_2$. A higher value of interaction energy (ΔE) corresponds to stronger adsorption.

3 Results and discussion

3.1 Geometries of $[BMIM]^+[PF_6]^-$, $[BMIM]^+[PF_6]^-$-DBT, $[BMIM]^+[PF_6]^-$-$DBTO_2$, $[BMIM]^+[BF_4]^-$, $[BMIM]^+[BF_4]^-$-DBT, and $[BMIM]^+[BF_4]^-$-$DBTO_2$

To investigate the structures of $[BMIM]^+[PF_6]^-/[BF_4]^-$ pairs, the $[PF_6]^-/[BF_4]^-$ anions were added to the corresponding C2-H2, C4-H4, and C5-H5 of vicinity of imidazolium ring. For comparison, $[PF_6]^-/[BF_4]^-$ anions around the alkyl side chains were taken into consideration. The most stable structures of $[BMIM]^+[PF_6]^-/[BF_4]^-$ are shown in Figure 3((a) and (d)). The most stable structure of $[BMIM]^+[PF_6]^-$ has seven F ⋯ H interactions, while the most stable structure of $[BMIM]^+[BF_4]^-$ has four F ⋯ H interactions. Hydrogen bonds occur between fluorine atoms on $[PF_6]^-/[BF_4]^-$ anions and C2-H2 as well as the hydrogen atoms on the adjacent alkyl side chains of $[BMIM]^+$ cation. Among all the interactions, the shortest hydrogen bonds (0.199 4 nm in $[BMIM]^+[PF_6]^-$ and 0.184 4 nm in $[BMIM]^+[BF_4]^-$) are to the C2-H2. A single hydrogen atom may participate in two or three hydrogen bonds. This type of bonding is called "bifurcated hydrogen bonding (three centered hydrogen bonding)" or "trifurcated hydrogen bonding (four centered hydrogen bonding)"[28,29]. The results show that H71 and H2 in $[BMIM]^+[PF_6]^-$ are involved in the formation of bifurcated hydrogen bonding and trifurcated hydrogen bonding, respectively, demonstrating that C2-proton plays a crucial role in the interactions between $[BMIM]^+$ and $[PF_6]^-$. The F⋯H contacts within the bifurcated hydrogen bonds and trifurcated hydrogen bonds are found to be unequivalent in terms of the different F⋯H distances. These deviations from linearity of the C-H⋯F angles are common for bifurcated hydrogen bonds and trifurcated hydrogen bonds. Our calculated results are in agreement with the reported conclusions that the presence of the hydrogen bonds between the acidic hydrogen (H2) and $[PF_6]^-/[BF_4]^-$ anions influences the structures of $[BMIM]^+[PF_6]^-/[BF_4]^-$.

The most stable $[BMIM]^+[PF_6]^-$-DBT, $[BMIM]^+[PF_6]^-$-$DBTO_2$, $[BMIM]^+[BF_4]^-$-DBT, and $[BMIM]^+[BF_4]^-$-$DBTO_2$ are shown in Figure 3((b), (c), (e) and (f)). The similar results of the strongest hydrogen bonds between one fluorine atom on $[PF_6]^-/[BF_4]^-$ anions and C2-H2 hydrogen atom on imidazolium ring are obtained for $[BMIM]^+[PF_6]^-$-DBT and $[BMIM]^+[BF_4]^-$-DBT. In the $[BMIM]^+[PF_6]^-$-DBT, the interacting distances between $[BMIM]^+[PF_6]^-$ and DBT are 0.296 8 nm (C8′⋯H61), 0.240 8 nm (F3⋯H9′), 0.259 0 nm (F2⋯H1′), 0.365 7 nm (N3⋯C9′), 0.358 7 nm (C4⋯C13′), 0.362 0 nm (N1⋯C11′), 0.383 9 nm (C5 ⋯ S5), 0.288 2 nm (H71 ⋯ C2′), and 0.312 3 nm (H91⋯C2′). As indicated in Figure 3(e), the interactions between $[BMIM]^+[BF_4]^-$ and DBT are H61 ⋯ C8′ (0.304 0 nm), F5 ⋯ H9′ (0.269 7 nm), F3⋯H9′ (0.252 7 nm), F3⋯H1′ (0.239 2 nm), N3⋯C9′ (0.361 9 nm), H71⋯C1′ (0.300 7 nm), C4⋯C10′ (0.355 1 nm, C5⋯C11′ (0.363 0 nm), H91⋯C2′ (0.322 0 nm), and H81 ⋯C3′ (0.298 5 nm). In both $[BMIM]^+[PF_6]^-$-DBT and $[BMIM]^+[BF_4]^-$-DBT, the $[BMIM]^+$ ring and DBT ring planes are parallel to each other, implying that the π-π interactions may occur. The π stacking (also called π-π stacking) refers to attractive, non-covalent interactions between aromatic rings[30,31]. The face-face stacked, edge-face stacked, and offset stacked geometries are three representative conformations of π-π interactions. As shown in Figure 3((b) and (e)), the offset parallel stacking interactions between [BMIM] ring and DBT ring in the gas phase occur. The offset stacked interactions are dependent on the orientation of the rings and it seems that H1′ and H9′ involved F2⋯H1′ and F3⋯H9′ interactions in $[BMIM]^+[PF_6]^-$-DBT as well as F3⋯H1′ and F5⋯H9′ interactions in $[BMIM]^+[BF_4]^-$-DBT may pronouncedly influence the formation of π-π interactions.

Through comparing the optimized structures of $[BMIM]^+[PF_6]^-$-DBT, $[BMIM]^+[PF_6]^-$-$DBTO_2$, $[BMIM]^+[BF_4]^-$-DBT, and $[BMIM]^+[BF_4]^-$-$DBTO_2$, we can find the significant differences between $[BMIM]^+[PF_6]^-$-DBT and $[BMIM]^+[PF_6]^-$-$DBTO_2$ as well as $[BMIM]^+[BF_4]^-$-DBT and $[BMIM]^+[BF_4]^-$-$DBTO_2$. The $DBTO_2$ rings are not parallel to the $[BMIM]^+$ rings. The oxygen atoms of $DBTO_2$ are competitive with fluorine atoms of $[PF_6]^-/[BF_4]^-$ anions to interact with hydrogen atoms to form hydrogen bonds. The interacting distances of H⋯O hydrogen bonds are 0.233 1 nm (H2 ⋯ O1), 0.263 3 nm (H81 ⋯ O1) and 0.236 5 nm (H62 ⋯ O2) in $[BMIM]^+[PF_6]^-$-$DBTO_2$ and 0.231 0 nm (H62 ⋯ O2) in $[BMIM]^+[BF_4]^-$-$DBTO_2$. The H ⋯ F hydrogen bonding interactions of H4′⋯F1 and H4′⋯F3 in $[BMIM]^+[PF_6]^-$-$DBTO_2$ as well as H7′⋯F1, H6′ ⋯F3 and H6′⋯F4 in $[BMIM]^+[BF_4]^-$-$DBTO_2$ occur.

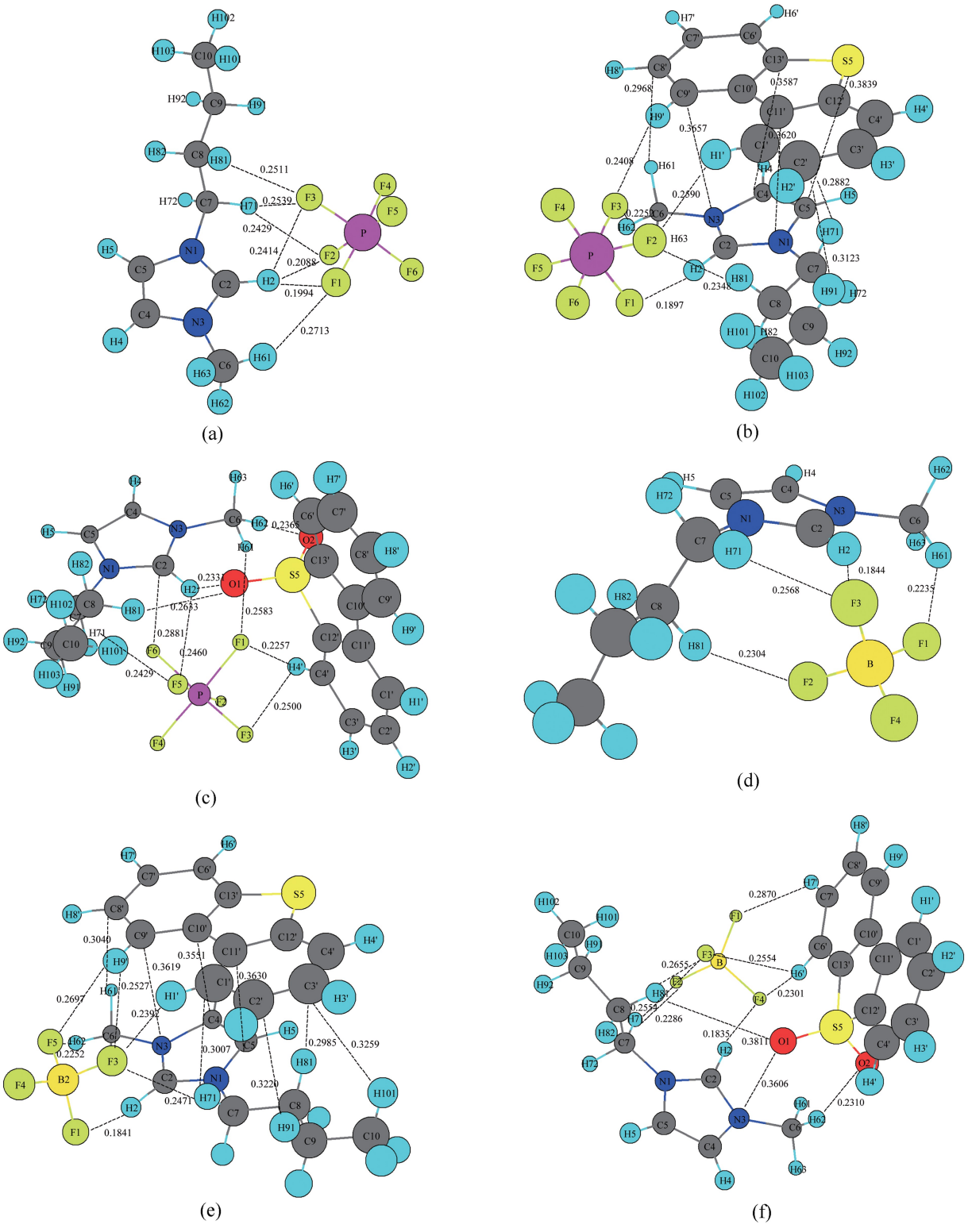

Figure 3　Optimized structures and some interaction distances (nm) of
(a): $[BMIM]^+[PF_6]^-$; (b): $[BMIM]^+[PF_6]^-$-DBT; (c): $[BMIM]^+[PF_6]^-$-$DBTO_2$;
(d): $[BMIM]^+[BF_4]^-$; (e): $[BMIM]^+[BF_4]^-$-DBT; (f): $[BMIM]^+[BF_4]^-$-$DBTO_2$

3.2　Interaction energies

On the basis of the optimized structures of $[BMIM]^+[PF_6]^-$, $[BMIM]^+[BF_4]^-$, $[BMIM]^+[PF_6]^-$-DBT, $[BMIM]^+[PF_6]^-$-$DBTO_2$, $[BMIM]^+[BF_4]^-$-DBT, $[BMIM]^+[BF_4]^-$-$DBTO_2$, DBT, and $DBTO_2$, the calculated interaction energies of $[BMIM]^+[PF_6]^-$-DBT, $[BMIM]^+[PF_6]^-$-$DBTO_2$, $[BMIM]^+[BF_4]^-$-DBT, and $[BMIM]^+[BF_4]^-$-

$DBTO_2$ are 15.92, 17.96, 9.69, and 11.72 kcal/mol, respectively, indicating that the interaction energies between $[BMIM]^+[PF_6]^-$/$[BMIM]^+[BF_4]^-$ and $DBTO_2$ are larger than that between $[BMIM]^+[PF_6]^-$/$[BMIM]^+[BF_4]^-$ and DBT, the interactions between $[BMIM]^+[PF_6]^-$ and DBT/$DBTO_2$ are stronger than that of between $[BMIM]^+[BF_4]^-$ and DBT/$DBTO_2$. Current results are consistent with the experimental results of Lo et al[2] The higher extraction capacity of $[BMIM]^+[PF_6]^-$ than that of $[BMIM]^+[BF_4]^-$ may be ascribed to the more fluorine atoms interacted with DBT/$DBTO_2$, while the stronger interactions between $[BMIM]^+[PF_6]^-$/$[BMIM]^+[BF_4]^-$ and $DBTO_2$ than that between $[BMIM]^+[PF_6]^-$/$[BMIM]^+[BF_4]^-$ and DBT may be assigned to the oxygen involved hydrogen bonds and higher polarity of $DBTO_2$. The dipole moments of $DBTO_2$ and DBT are 5.62 and 0.76 D, respectively. The polarity of $DBTO_2$ is larger than that of DBT, so $DBTO_2$ is readily remained in the ionic liquid phase, being able to enhance the extraction efficiency of the extraction-oxidation system.

3.3 NBO analysis

The optimized structures were employed for NBO analysis at B3LYP/6-31++G** level. The NBO analysis involves population analysis that pertains to localized wave functions properties. The NBO analysis were performed for the DBT, $DBTO_2$, $[BMIM]^+[PF_6]^-$, $[BMIM]^+[PF_6]^-$-DBT, $[BMIM]^+[PF_6]^-$-$DBTO_2$, $[BMIM]^+[BF_4]^-$, $[BMIM]^+[BF_4]^-$-DBT, and $[BMIM]^+[BF_4]^-$-$DBTO_2$. It is clear that the DBT, $DBTO_2$ adsorptions on $[BMIM]^+[PF_6]^-$/$[BF_4]^-$ influence the distribution of their charges. Compared with the NBO charges, the hydrogen atoms involved hydrogen bonds are more positive. The shorter the contacts of hydrogen bonds, the more positive the charges of hydrogen atoms are.

Hydrogen bonds are commonly accepted in chemistry as distinct interactions. However, the definition of hydrogen bond is somewhat arbitrary. Geometric, energetic and spectroscopic criteria have been used to classify them into strong, moderate and weak, but the limits between such categories are diffuse[32]. Nowadays it seems quite well accepted that hydrogen bonding influences the structures of ionic liquids. The aim of this section is to discern the extent of hydrogen bonding contacts by using NBO analysis results.

Table 1 lists the donor-acceptor NBO interactions in $[BMIM]^+[PF_6]^-$, $[BMIM]^+[PF_6]^-$-DBT, $[BMIM]^+[PF_6]^-$-$DBTO_2$, $[BMIM]^+[BF_4]^-$, $[BMIM]^+[BF_4]^-$-DBT, $[BMIM]^+[BF_4]^-$-$DBTO_2$, and their $E(2)$ values. The extent of electron delocalization from donors to acceptors can be evaluated by analyzing the second-order perturbation stabilization energy $E(2)$, which indicates the intensity of the interactions between the orbitals of the electron donors and acceptors. The higher the value of $E(2)$, the more electrons are transferred from the donor orbitals to acceptor orbitals. As indicated in Table 1, the C2-proton involved hydrogen bonds are strongest, in terms of the large $E(2)$ of 9.05 kcal/mol in $[BMIM]^+[PF_6]^-$ (LP(F1)→σ*(C2-H2)), 15.03 kcal/mol in $[BMIM]^+[PF_6]^-$-DBT (LP(F1)→σ*(C2-H2)), 3.65 kcal/mol in $[BMIM]^+[PF_6]^-$-$DBTO_2$(LP(O1)→σ*(C2-H2)), 13.55 kcal/mol in $[BMIM]^+[BF_4]^-$ (LP(F3)→σ*(C2-H2)), 15.94 kcal/mol in $[BMIM]^+[BF_4]^-$-DBT (LP(F1)→σ*(C2-H2)), and 16.09 kcal/mol in $[BMIM]^+[BF_4]^-$-$DBTO_2$ (LP(F4)→σ*(C2-H2)), in agreement with their short O···H contacts. The interaction energies listed in Table 1 and their corresponding distances displayed in Figure 3 demonstrate that the shorter the contact is, the larger the value of $E(2)$ is. The interaction energies of LP(O2)→σ*(C6-H62), LP(O1)→σ*(C8-H81), LP(O1)→π*(N1-C2) in $[BMIM]^+[PF_6]^-$-$DBTO_2$ and LP(O2)→σ*(C6-H62) in $[BMIM]^+[BF_4]^-$-$DBTO_2$ are 3.09, 0.58, 0.20, and 3.31 kcal/mol, respectively, showing the strong O···H interactions between $[BMIM]^+[PF_6]^-$/$[BF_4]^-$ and $DBTO_2$. The interactions of π(C5-C4)→π*(C10′-C9′), π(C10′-C9′)→π*(N1-C2), π(C5-C4)→π*(C13′-C6′), π*(C5-C4)→π*(C13′-C6′), π(C12′-C11′)→π*(C5-C4), π(C13′-C6′)→π*(C5-C4) in $[BMIM]^+[PF_6]^-$-DBT, π(C5-C4)→π*(C10′-C9′), π(C5-C4)→π*(C12′-C11′), π(C8′-C7′)→π*(C5-C4), π(C5-C4)→π*(C13′-C6′), π(C12′-C11′)→π*(C5-C4), π(C13′-C6′)→π*(C5-C4) in $[BMIM]^+[BF_4]^-$-DBT imply that π-π interactions between $[BMIM]^+[PF_6]^-$/$[BF_4]^-$ and DBT occur.

Based on these calculations, it may be concluded that the HOMOs (highest occupied molecular orbitals) of $[BMIM]^+[PF_6]^-$-DBT, $[BMIM]^+[PF_6]^-$-$DBTO_2$, $[BMIM]^+[BF_4]^-$-DBT, $[BMIM]^+[BF_4]^-$-$DBTO_2$ come from πorbitals of DBT/$DBTO_2$, the LUMOs (lowest unoccupied molecular orbitals) is mainly derived from π* orbitals of DBT/$DBTO_2$ spreading over the rings.

3.4 AIM analysis

The theory of AIM has been applied theoretically to a wide variety of structures containing different

types of hydrogen interactions; these interactions can be successfully described by means of topological properties of electron density distribution $\rho(r)$ with AIM2000. The electron density at the bond critical point provides a measure of the strength of the bonding between two atoms. According to Bader's topological AIM theory[33], the chemical bonds can be illustrated in terms of the total electronic density $\rho(r)$ and its corresponding Laplacian $\nabla^2\rho(r)$ that is the sum of three eigenvalues of the Hessian matrix of $\rho(r)$ ($\nabla^2\rho(r) = \lambda_1 + \lambda_2 + \lambda_3$). The topological properties of electron density (ρ), Laplacian of density ($\nabla^2\rho$), eigenvalues of the Hessian matrix (λ_1, λ_2, λ_3) of DBT, $DBTO_2$, $[BMIM]^+[PF_6]^-$, $[BMIM]^+[PF_6]^-$-DBT, $[BMIM]^+[PF_6]^-$-$DBTO_2$, $[BMIM]^+[BF_4]^-$, $[BMIM]^+[BF_4]^-$-DBT, and $[BMIM]^+[BF_4]^-$-$DBTO_2$ were analyzed. In the case of interactions, the bond path with bond critical point should exist. According to this criterion, the interactions are displayed in Figure 3. The Laplacian $\nabla^2\rho$ of the bond critical points is positive, demonstrating the nature of closed shell interactions. The large values of electronic density and Laplacian of interactions are consistent with the short distances, showing a clear relationship between the topological properties of the charge density with the inter-nuclear distances of the systems.

Table 1　Some donor-acceptor interactions in $[BMIM]^+[PF_6]^-$, $[BMIM]^+[PF_6]^-$-DBT, $[BMIM]^+[PF_6]^-$-$DBTO_2$, $[BMIM]^+[BF_4]^-$, $[BMIM]^+[BF_4]^-$-DBT, $[BMIM]^+[BF_4]^-$-$DBTO_2$ and their second order perturbation stabilization energies, E(2) (kcal/mol)

Donor	Acceptor	$E(2)$ /(kcal·mol^{-1})	Donor	Acceptor	$E(2)$ /(kcal·mol^{-1})
		$[BMIM]^+[PF_6]^-$			
LP(F2)	σ*(C2-H2)	5.63	LP(F2)	σ*(C7-H71)	2.26
LP(F1)	σ*(C2-H2)	9.05	LP(F2)	σ*(N3-C2)	0.13
LP(F3)	σ*(C2-H2)	0.74	LP(F3)	σ*(C8-H81)	0.39
LP(F3)	σ*(C7-H71)	0.43	LP(F3)	π*(N1-C2)	0.14
LP(F1)	σ*(C6-H61)	0.21			
		$[BMIM]^+[PF_6]^-$-DBT			
π(C5-C4)	π*(C10′-C9′)	0.08	π(C5-C4)	π*(C13′-C6′)	0.09
LP(F2)	σ*(C1-H1′)	0.69	π*(C5-C4)	π*(C13′-C6′)	0.06
π(C4′-C3′)	σ*(C7-H71)	0.45	π(C12′-C11′)	π*(C5-C4)	0.20
π(C12′-C11′)	σ*(C7-H71)	0.10	π(C1′-C2′)	σ*(C7-H71)	0.26
π(C1′-C2′)	σ*(C8-H81)	0.09	π(C1′-C2′)	σ*(C9-H91)	0.13
π(C10′-C9′)	π*(N1-C2)	0.06	π(C13′-C6′)	π*(C5-C4)	0.11
π(C8′-C7′)	σ*(C6-H61)	0.48	LP(S)	π*(C5-C4)	0.16
LP(S)	σ*(C5-H51)	0.11	LP(F3)	σ*(C2-H2)	0.39
LP(F3)	σ*(C6-H62)	2.24	LP(F3)	σ*(C6-H63)	0.07
LP(F3)	π*(N1-C2)	0.39	LP(F2)	σ*(C8-H81)	2.55
LP(F3)	σ*(C9-H9′)	0.97	LP(F1)	σ*(C2-H2)	15.03
		$[BMIM]^+[PF_6]^-$-$DBTO_2$			
LP(F1)	σ*(C6-H61)	0.16	σ(S5-O1)	RY*(H81)	0.41
LP(O2)	σ*(C6-H62)	3.09	LP(O2)	RY*(H62)	0.21
LP(O1)	σ*(C2-H2)	3.65	LP(O1)	σ*(C8-H81)	0.58
LP(O1)	RY*(H2)	0.32	LP(O1)	π*(N1-C2)	0.20
σ*(S5-O2)	σ*(C6-H62)	0.23	σ*(S5-O1)	σ*(C2-H2)	0.26
σ*(S5-O1)	σ*(C8-H81)	0.34	LP(F6)	σ*(C7-H71)	0.12
LP(F5)	π*(N1-C2)	0.26	LP(F6)	π*(N1-C2)	0.53
LP(F1)	σ*(C4′-H4′)	3.47	LP(F1)	RY*(H4′)	0.33
LP(F1)	σ*(C2-H2)	0.37	LP(F1)	π*(N1-C2)	0.47
LP(F3)	σ*(C4′-H4′)	0.66	LP(F1)	RY*(H61)	0.10
LP(F5)	σ*(C7-H71)	1.05	LP(F5)	σ*(C2-H2)	0.95

Continued table

Donor	Acceptor	$E(2)$ /(kcal·mol^{-1})	Donor	Acceptor	$E(2)$ /(kcal·mol^{-1})
		[BMIM]$^+$[BF_4]$^-$			
LP(F1)	σ*(C2-H2)	0.73	LP(F1)	σ*(C6-H61)	2.96
LP(F3)	σ*(C2-H2)	13.55	LP(F3)	σ*(C7-H71)	0.90
LP(F2)	σ*(C8-H81)	2.07			
		[BMIM]$^+$[BF_4]$^-$-DBT			
π(C5-C4)	π*(C10′-C9′)	0.25	π(C5-C4)	π*(C13′-C6′)	0.10
π(C5-C4)	π*(C12′-C11′)	0.19	π(C4′-C3′)	σ*(C10-H101)	0.09
π(C4′-C3′)	σ*(C8-H81)	0.44	π(C12′-C11′)	π*(C5-C4)	0.23
		[BMIM]$^+$[BF_4]$^-$-DBT			
π(C12′-C11′)	σ*(C8-H81)	0.10	π(C1′-C2′)	σ*(C7-H71)	0.31
π(C1′-C2′)	σ*(C9-H91)	0.13	π(C13′-C6′)	π*(C5-C4)	0.12
π(C13′-C6′)	σ*(C4-H4)	0.05	π(C8′-C7′)	σ*(C6-H61)	0.33
π(C8′-C7′)	π*(C5-C4)	0.09	LP(S)	σ*(C5-H5)	0.09
LP(F1)	σ*(C2-H2)	15.94	LP(F5)	σ*(C6-H62)	2.80
LP(F3)	σ*(C7-H71)	1.15	LP(F5)	π*(N1-C2)	0.17
LP(F3)	π*(N1-C2)	0.23	LP(F5)	σ*(C9′-H9′)	0.14
LP(F3)	σ*(C1′-H1′)	1.25	LP(F4)	π*(N1-C2)	0.05
LP(F3)	σ*(C9′-H9′)	0.73	LP(F4)	σ*(C2-H2)	0.19
		[BMIM]$^+$[BF_4]$^-$-$DBTO_2$			
LP(F1)	σ*(C7′-H7′)	0.23	LP(F1)	σ*(C2-H2)	0.49
LP(F1)	σ*(C7-H71)	0.10	LP(F3)	π*(C6′-C13′)	0.12
LP(F3)	σ*(C6′-H6′)	0.21	LP(F3)	σ*(C8-H81)	0.21
LP(F3)	σ*(C7-H72)	0.06	LP(F3)	σ*(C7-H71)	0.24
LP(F3)	σ*(C8-H82)	0.06	LP(F3)	σ*(C9-H91)	0.05
LP(F4)	σ*(C6′-H6′)	2.45	LP(F4)	σ*(C2-H2)	16.09
LP(F4)	π*(N1-C2)	0.05	LP(F4)	σ*(N1-C2)	0.06
LP(F4)	σ*(C7-H71)	0.05	LP(F2)	σ*(C6′-H6′)	0.10
LP(F2)	σ*(C7-H71)	3.00	LP(F2)	σ*(C2-H2)	0.05
LP(O2)	σ*(C6-H62)	3.31	LP(O2)	RY*(H62)	0.26
σ*(S5-O2)	σ*(C6-H62)	0.19	LP(O1)	RY*(N1)	0.06

The interactions between [BMIM]$^+$[PF_6]$^-$ and DBT/$DBTO_2$ as well as [BMIM]$^+$[BF_4]$^-$ and DBT/$DBTO_2$, e. g. C5⋯S5 (ρ= 0.003 84 au, $\nabla^2\rho$= 0.011 40 au), N3⋯C9′ (ρ= 0.003 45 au, $\nabla^2\rho$= 0.010 26 au) and N3⋯C11′ (ρ= 0.003 68 au, $\nabla^2\rho$ = 0.011 40 au) in [BMIM]$^+$[PF_6]$^-$ - DBT as well as C10′ ⋯ C4-C5 (ρ = 0.005 66 au, $\nabla^2\rho$ = 0.014 14 au) and N3-C9′ (ρ= 0.003 93 au, $\nabla^2\rho$= 0.011 45 au) in [BMIM]$^+$[BF_4]$^-$ - DBT, are remarkably different, indicating the occurrence of π-π interactions between [BMIM]$^+$[PF_6]$^-$/[BF_4]$^-$ and DBT. The topological properties of the oxygen atoms involved bond critical points of O2 ⋯ H62 (ρ= 0.011 10 au, $\nabla^2\rho$= 0.034 97 au), O1⋯H22 (ρ= 0.012 03 au, $\nabla^2\rho$= 0.039 51 au) and O1⋯H81 (ρ = 0.005 75 au, $\nabla^2\rho$= 0.021 90 au) in [BMIM]$^+$[PF_6]$^-$-$DBTO_2$ as well as O2⋯H62 (ρ= 0.013 02 au, $\nabla^2\rho$= 0.040 33 au), O1⋯N3 (ρ= 0.002 81 au, $\nabla^2\rho$= 0.011 04 au) and O1⋯H81 (ρ = 0.000 55 au, $\nabla^2\rho$= 0.002 35 au) in [BMIM]$^+$[BF_4]$^-$-$DBTO_2$ demonstrate that oxygen atoms involved interactions may play a vital role in the interactions between [BMIM]$^+$[PF_6]$^-$/[BF_4]$^-$ and $DBTO_2$, resulting in the larger interaction energies of [BMIM]$^+$[PF_6]$^-$/[BF_4]$^-$-$DBTO_2$ in comparison to those of corresponding [BMIM]$^+$[PF_6]$^-$/[BF_4]$^-$-DBT. The changes of topological properties of ring critical points may be ascribed to the interactions between [BMIM]$^+$[PF_6]$^-$/[PF_6]$^-$ and DBT/$DBTO_2$.

AIM theory can not only indicate the nature of interactions, but also describe the strength of hydrogen bonds through the electron density[34]. The strength of any pair of interacting atoms is reflected by the electron density at the corresponding bond critical point. An exponential dependence on d(H⋯

O) is observed for the values of the second derivatives of ρat the BCPs of hydrogen bonds[35,36]. Relationships between the distances d(F⋯H) and their corresponding ln(ρ_b) have been established. Figure 4 displays the plots of the distances of d(F⋯H) versus their corresponding ln(ρ_b). The correlation coefficients for [BMIM]$^+$[PF_6]$^-$, [BMIM]$^+$[PF_6]$^-$-DBT, [BMIM]$^+$[PF_6]$^-$-$DBTO_2$, [BMIM]$^+$[BF_4]$^-$, [BMIM]$^+$[BF_4]$^-$-DBT, and [BMIM]$^+$[BF_4]$^-$-$DBTO_2$ are 0.992, 0.956, 0.994, 0.999, 0.999 and 0.994, respectively, demonstrating the good relation between hydrogen bonding strengths and their distances. The topological properties are useful descriptors for the strength of hydrogen bonds.

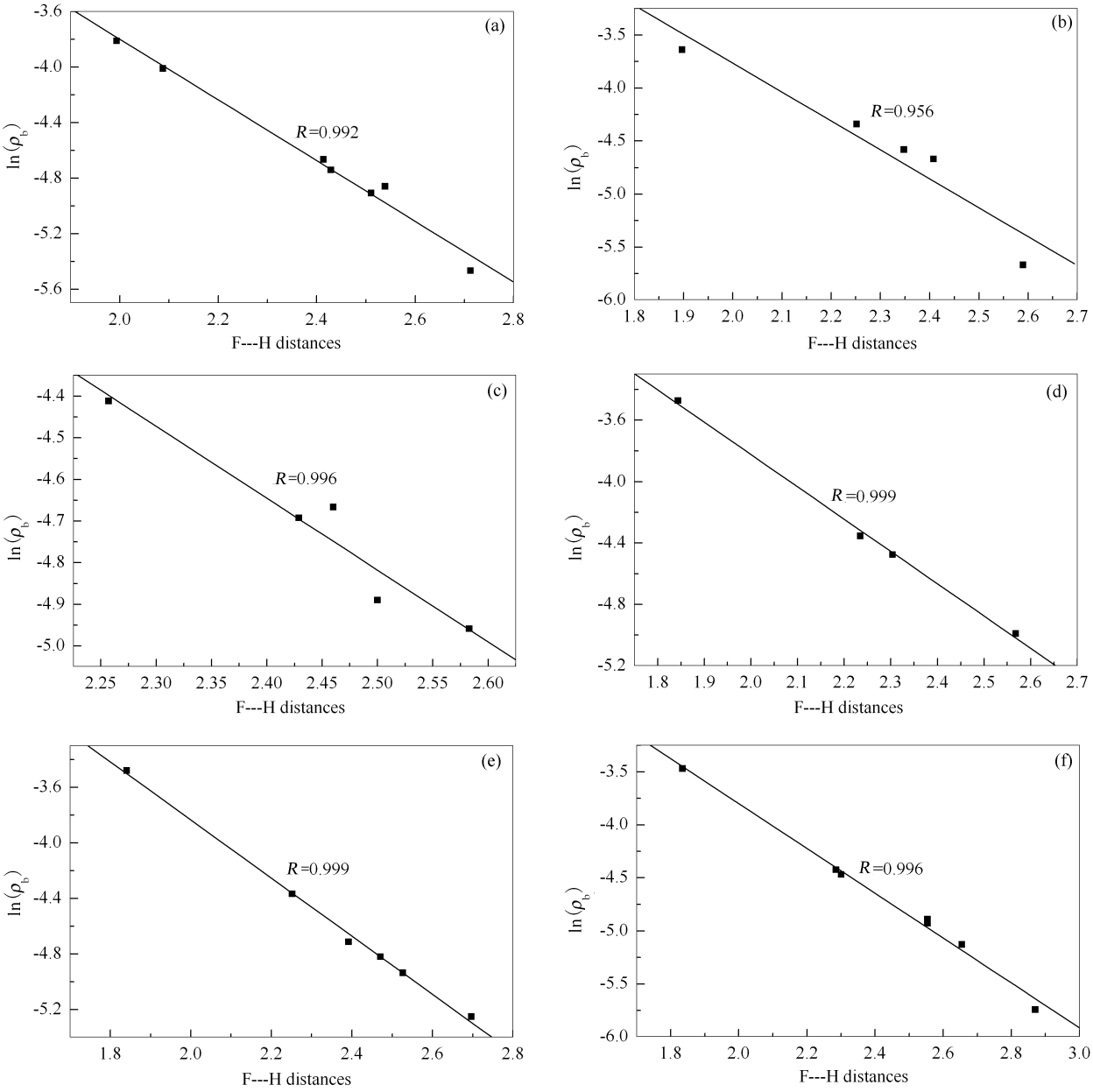

Figure 4　Linear correlations between the F⋯H distances and their corresponding ln(ρ_b) of (a): [BMIM]$^+$[PF_6]$^-$; (b): [BMIM]$^+$[PF_6]$^-$-DBT; (c): [BMIM]$^+$[PF_6]$^-$-$DBTO_2$; (d): [BMIM]$^+$[BF_4]$^-$; (e): [BMIM]$^+$[BF_4]$^-$-DBT; (f): [BMIM]$^+$[BF_4]$^-$-$DBTO_2$

4 Conclusions

We have investigated the interactions between DBT/$DBTO_2$ and [BMIM]$^+$[PF_6]$^-$/[BMIM]$^+$[BF_4]$^-$ at GGA/PW91/DNP level. The most stable optimized structures of [BMIM]$^+$[PF_6]$^-$-DBT, [BMIM]$^+$[PF_6]$^-$-$DBTO_2$, [BMIM]$^+$[BF_4]$^-$-DBT, and [BMIM]$^+$[BF_4]$^-$-$DBTO_2$ were obtained by

NBO and AIM analyses. The optimized structures of $[BMIM]^+[PF_6]^-$-DBT and $[BMIM]^+[BF_4]^-$-DBT suggest that the DBT rings are parallel to the rings of the imidazolium cations, indicating the occurrence of π-π interactions as corroborated by NBO and AIM analyses. In the structures of $[BMIM]^+[PF_6]^-$-$DBTO_2$ and $[BMIM]^+[BF_4]^-$-$DBTO_2$, the oxygen atoms of $DBTO_2$ tend to locate near C2-proton and methyl group of $[BMIM]^+$, while hydrogen atoms of $DBTO_2$ are inclined to close fluorine atoms on $[PF_6]^-$/$[BF_4]^-$ anions to form F⋯H interactions. The interaction energies between $DBTO_2$ and $[BMIM]^+[PF_6]^-$/$[BMIM]^+[BF_4]^-$ are larger than that of DBT and $[BMIM]^+[PF_6]^-$/$[BMIM]^+[BF_4]^-$, due to the oxygen involved interactions.

References

[1] BOSMANN A, DATSEVICH L, JESS A, LAUTER A, SCHMITZ C, WASSEERSCHEID P. Deep desulfurization of diesel fuel by extraction with ionic liquids[J]. Chem Commun, 2001, **23**(23): 2494-2495.

[2] LO W-H, YANG H-Y, WEI G-T. One-pot desulfurization of light oils by chemical oxidation and solvent extraction with room temperature ionic liquids[J]. Green Chem, 2003, **5**(5): 639-642.

[3] WANG J-L, ZHAO D-S, ZHOU E-P, DONG Z. Desulfurization of gasoline by extraction with *N*-alkyl-pyridinium-based ionic liquids[J]. J Fuel Chem Technol, 2007, **35**(3): 293-296.

[4] ZHANG C, WANG F, PAN X-Y, LIU X-Q. Study of extraction-oxidation desulfurization of model oil by acidic ionic liquid[J]. J Fuel Chem Technol, 2011, **39**(9): 689-693.

[5] ANANTHARAJ R, BANERJEE T. Phase behavior of 1-ethyl-3-methylimidazolium thiocyanate ionic liquid with catalytic deactivated compounds and water at several temperatures: Experiments and theoretical predictions[J]. Int J Chem Eng, 2011, **2011**(1):1-13.

[6] KUMAR A A P, BANERJEE T. Thiophene separation with ionic liquids for desulphurization: A quantum chemical approach[J]. Fluid Phase Equilib, 2009, **278**(1/2): 1-8.

[7] ANANTHARAJ R, BANERJEE T. Liquid-liquid equilibria for quaternary systems of imidazolium based ionic liquid + thiophene + pyridine + iso-octane at 298.15 K: Experiments and quantum chemical predictions[J]. Fluid Phase Equilib, 2011, **312**(1): 20-30.

[8] SANTIAGO R S, SANTOS G R, AZNAR M. UNIQUAC correlation of liquid-liquid equilibrium in systems involving ionic liquids: the DFT-PCM approach[J]. Fluid Phase Equilib, 2009, **278**(1/2): 54-61.

[9] HANKE C G, JOHANSSON A, HARPER J B, LYNDEN-BELL R M. Why are aromatic compounds more soluble than aliphatic compounds in dimethylimidazolium ionic liquids? A simulation study[J]. Chem Phys Lett, 2003, **374**(1/2): 85-90.

[10] KEDRA-KROLIK K, FABRICE M, JAUBERT J. Extraction of thiophene or pyridine from *n*-heptane using ionic liquids, gasoline and diesel desulfurization[J]. Ind Eng Chem Res, 2011, **50**(4): 2296-2306.

[11] ANANTHARAJ R, BANERJEE T. Quantum chemical studies on the simultaneous interaction of thiophene and pyridine with ionic liquids[J]. AIChE J, 2011, **57**(3): 749-764.

[12] LU R, QU Z, YU H, WANG F, WANG S. Comparative study on interactions between ionic liquids and pyridine/hexane[J]. Chem Phys Lett, 2012, **532**(4): 13-18.

[13] DONG K, ZHANG S, WANG D, YAO X. Hydrogen bonds in imidazolium ionic liquids[J]. J Phys Chem A, 2006, **110**(31): 9775-9782.

[14] HEIMER N E, del SESTO R E, MENG Z, WILKES J S, CARPER W R. Vibrational spectra of imidazolium tetrafluoroborate ionic liquids[J]. J Mol Liq, 2006, **124**(1/3): 84-95.

[15] BHARGAVA B L, BALASUBRAMANIAN S. Insights into the structure and dynamics of a room-temperature ionic liquid: Ab initio molecular dynamics simulation studies of 1-n-butyl-3-methylimidazolium hexafluorophosphate ([bmim][PF_6]) and the [bmim][PF_6]-CO_2 mixture[J]. J Phys Chem B, 2007, **111**(17): 4477-4487.

[16] MORROW T I, MAGINN E J. Molecular dynamics study of the ionic liquid 1-n-butyl-3-methylimidazolium hexafluorophosphate[J]. J Phys Chem B, 2002, **106**(49): 12807-12813.

[17] KATSYUBA S A, DYSON P J, VANDYUKOVA E E, CHERNOVA A V, VIDIS A. Molecular structure, vibrational spectra, and hydrogen bonding of the ionic liquid 1-ethyl-3-methyl-1H-imidazolium tetrafluoroborate[J]. Helv Chim Acta, 2004, **87**(10): 2556-2565.

[18] MICAELO N M, BAPTISTA A M, SOARES C M. Parametrization of 1-butyl-3-methylimidazolium hexafluorophosphate/nitrate ionic liquid for the GROMOS force field[J]. J Phys Chem B, 2006, **110**(29): 14444-14451.

[19] TALATY E R, RAJA S, STORHAUG V J, DOLLE A, CARPER W R. Raman and infrared spectra and ab initio calculations of C_{2-4}MIM imidazolium hexafluorophosphate ionic liquids[J]. J Phys Chem B, 2004, **108**(35): 13177-13184.

[20] PERDEW J P, WANG Y. Accurate and simple analytic representation of the electron-gas correlation energy[J]. Phys Rev B, 1992, **45**(23): 13244-13249.

[21] DELLEY B. An all-electron numerical method for solving the local density functional for polyatomic molecules[J]. J Chem Phys, 1990, **92**(1): 508-517.

[22] DELLEY B. From molecules to solids with the $DMol^3$ approach[J]. J Chem Phys, 2000, **113**(18): 7756-7764.

[23] CASTELLANO O, GIMON R, SOSCUN H. Theoretical study of the σ-π and π-π interactions in heteroaromatic monocyclic molecular complexes of benzene, pyridine, and thiophene dimers: Implications on the resin-asphaltene stability in crude oil[J]. Energy Fuels, 2011, **25**(6): 2526-2541.

[24] REED A E, CURTISS L A, WEINHOLD F. Intermolecular interactions from a natural bond orbital, donor-acceptor viewpoint[J]. Chem Rev, 1988, **83**(6): 899-926.

[25] BIEGLER-KONIG F, SCHONBOHM J. Update of the AIM2000 program for atoms in molecules[J]. J Comput Chem, 2002, 23(15): 1489-1494.

[26] BIEGLER-KONIG F, SCHONBOHM J, BAYLES D. AIM2000 - A program to analyze and visualize atoms in molecules[J]. J Comput Chem, 2001, **22**(5): 545-559.

[27] INADA Y, ORITA H. Efficiency of numerical basis sets for predicting the binding energies of hydrogen bonded complexes: Evidence of small

basis set superposition error compared to Gaussian basis sets[J]. J Comput Chem, 2008, **29**(2): 225-232.
[28] ROZAS I, ALKORTA I, ELGUERO J. Bifurcated hydrogen bonds: three-centered interactions[J]. J Phys Chem A, 1988, **102**(48): 9925-9932.
[29] PADIYAR G S, SESHADRI T P. Trifurcated (four-center) hydrogen bond in solid state crystal structure of 5′-amino-5′-deoxyadenosine *p*-toluenesulfonate[J]. Nucleos Nucleot, 1996, **15**(4): 857-865.
[30] SINNOKROT M O, VALEEV E F, SHERRILL C D. Estimates of the ab initio limit for π-πinteractions: The benzene dimmer[J]. J Am Chem Soc, 2002, **124**(36): 10887-10893.
[31] HUNTER C A, SANDERS J K M. The nature of π-πinteractions[J]. J Am Chem Soc, 1990, **112**(14): 5525-5534.
[32] DESIRAJU G R. Hydrogen bridges in crystal engineering: Interactions without borders[J]. Acc Chem Res, 2002, **35**(7): 565-573.
[33] BADER R F W. A quantum theory of molecular structure and its applications[J]. Chem Rev, 1991, **91**(5): 893-928.
[34] CHECINSKA L, GRABOWSKI S J, MALECKA M. An analysis of bifurcated H-bonds: Crystal and molecular structures of *O*,*O*-diphenyl 1-(3-phenylthioureido) pentanephosphonate and *O*,*O*-diphenyl 1-(3-phenylthioureido) butanephosphonate[J]. J Phys Org Chem, 2003, **16**(4): 213-219.
[35] ESPINOSA E, SOUHASSOU M, LACHEKAR H, LECOMTE C. Topological analysis of the electron density in hydrogen bonds[J]. Acta Cryst, 1999, B**55**(4): 563-574.
[36] NETZEL J, van SMAALEN S. Topological properties of hydrogen bonds and covalent bonds from charge densities obtained by the maximum entropy method (MEM)[J]. Acta Cryst, 2009, B**56**(5): 624-638.

二苯并噻吩及其氧化物与离子液体相互作用的理论研究

吕仁庆[1], 林　进[2], 曲占庆[3]

(1. 中国石油大学(华东)理学院 化学系, 山东 青岛　266580;
2. 中国石油大学(华东) 化学工程学院, 山东 青岛　266580; 3. 中国石油大学(华东) 石油工程学院, 山东 青岛　266580)

摘　要: 采用密度泛函理论方法比较了 DBT/$DBTO_2$ 和[BMIM]$^+$[PF_6]$^-$/[BMIM]$^+$[BF_4]$^-$的相互作用。对最稳定的[BMIM]$^+$[PF_6]$^-$、[BMIM]$^+$[PF_6]$^-$-DBT、[BMIM]$^+$[PF_6]$^-$-$DBTO_2$、[BMIM]$^+$[BF_4]$^-$、[BMIM]$^+$[BF_4]$^-$-DBT、[BMIM]$^+$[BF_4]$^-$-$DBTO_2$ 进行了 NBO 和 AIM 分析。结果表明,DBT 和[BMIM]$^+$[PF_6]$^-$/[BMIM]$^+$[BF_4]$^-$中的咪唑环彼此相互平行,NBO 和 AIM 分析表明它们之间发生了π-π相互作用。H1′和 H9′形成的 F…H 氢键有利于π-π堆积作用的形成。$DBTO_2$ 倾向于趋近 C2-H2 和甲基基团形成 O…H 相互作用; $DBTO_2$ 优先吸附在[BMIM]$^+$[PF_6]$^-$/[BMIM]$^+$[BF_4]$^-$。在模拟油中,[BMIM]$^+$[PF_6]$^-$和[BMIM]$^+$[BF_4]$^-$离子液体对 $DBTO_2$ 的萃取能力大于 DBT,其原因是可能是 $DBTO_2$ 具有较大的极性和 O…H 与 F…H 的氢键作用。

关键词: 密度泛函理论; 二苯并噻吩; 二苯并噻吩氧化物; 离子液体
中图分类号: TE624　　**文献标识码:** A